Contributions, Geophysical Institute, Kyoto University, No. 12, 1972, 49–62

A COMPARISON OF SOME SCHEMES PARAMETERIZING CUMULUS CONVECTION BY NUMERICAL EXPERIMENTS

By

Haruo OHNISHI and Tomio ASAI

(Received September 6, 1972)

Abstract

Among those which parameterize cumulus convection, the "penetrative moist convection (PMC) scheme" and the "convective adjustment (CA) scheme" are compared with each other by applying them to a simple numerical model. A main difference between them appears in the vertical distribution of warming. The warming in the PMC scheme has characteristics of penetrative convection, whereas that in the CA scheme hardly penetrate into a stable layer. Features found in precipitations and stabilities for perturbations of different wavelengths are discussed as well as for each of the schemes. Some variations of these two schemes are also examined.

1. Introduction

It is well known that a number of tall convective clouds which are frequently called "hot towers" play the most important role in developing and maintaining a tropical cyclone (e.g., Riehl and Malkus [1961]). The latent heat release due to condensation of water vapor which depends primarily on cumulus convection must be taken into account in energy balance of the global atmosphere, especially in the tropics (e.g., Palmén and Newton [1969]). It is needless to say that the effect of cumulus convection cannot be neglected in most severe meso-scale phenomena.

For better understanding of the physical processes in the phenomena mentioned above, attempts to incorporate a total effect of cumulus convection in the dynamics of large-scale motion have been made by many investigators (e.g., Ooyama [1963], Charney and Eliassen [1964], Manabe *et al.* [1965], Asai and Kasahara [1967] and Arakawa *et al.* [1968]).

The purpose of the present study is to compare characteristics of the schemes parameterizing cumulus convection with one another by applying them to a simple numerical model.

2. Basic equations

2.1 Governing equations

Governing equations are described in the x-, y- and p- (pressure) coordinate system, where x-, y- and p-coordinates are directed eastward, northward and downward

respectively. The model atmosphere is divided into six layers and the physical quantities are defined in a manner shown in Fig. 1. Consider a small amplitude perturba-

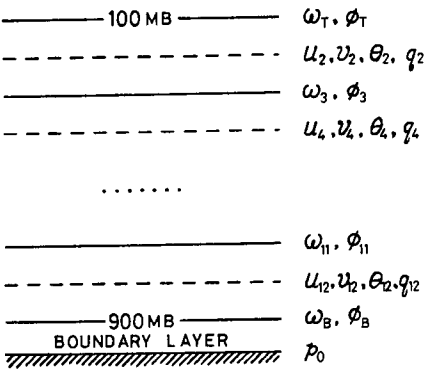

Fig. 1. The 6-layer model. The physical quantities are defined at the levels as indicated in the right side.

tion superimposed on a still atmosphere in a hydrostatic equilibrium. Assuming the perturbation independent of the y-coordinate, we may write the perturbation equations as follows.

$$\frac{\partial u}{\partial t}-fv=-\frac{\partial \phi}{\partial x}, \tag{2.1}$$

$$\frac{\partial v}{\partial t}+fu=0, \tag{2.2}$$

$$\frac{\partial \phi}{\partial p}=-\frac{R\pi^*}{p}\theta, \tag{2.3}$$

$$\frac{\partial u}{\partial x}+\frac{\partial \omega}{\partial p}=0, \tag{2.4}$$

$$\frac{\partial \theta}{\partial t}+\omega\frac{\partial \Theta}{\partial p}=\frac{1}{c_p\pi^*}(\dot{Q}+\dot{Q}_c), \tag{2.5}$$

$$\frac{\partial q}{\partial t}+\omega\frac{\partial \bar{q}}{\partial p}=-\frac{\dot{Q}}{L}+\dot{q}_c, \tag{2.6}$$

where $\pi^*=(p/p_0)^{R/c_p}$. u, v and ω are the perturbation velocity components in the x-, y- and p-directions respectively, ϕ the geopotential, θ the potential temperature and q the specific humidity of the perturbations. The potential temperature and the specific humidity of the basic field are denoted by Θ and $\bar{q}$ respectively. f, R, c_p, L and p_0 are the Coriolis parameter, the specific gas constant of dry air, the specific heat at constant pressure, the latent heat of condensation of water vapor and the reference pressure respectively. In Eqs. (2.5) and (2.6) $\dot{Q}$ is the heating term due to release of latent heat by the perturbation, while $\dot{Q}_c$ and $\dot{q}_c$ indicate the effects of

condensation of the water vapor through cumulus convection on the temperature and the moisture fields respectively. The condensed water vapor is assumed to precipitate out of the system instantaneously, and the cooling due to the re-evaporation of water droplets which may be suspended in the air is not taken into account.

In this study we investigate characteristics of each scheme to be shown in the tropical region where no strong baroclinicity exists. Two types of basic states are selected. In Case A the mean soundings of the West Indies during hurricane seasons (Jul.~Oct.) analysed by Jordan [1958] are employed for the basic state of Θ and $\bar{q}$, and in Case B more destabilized basic state is assumed as drawn in Fig. 2. The reason for taking these two basic states is given in Section **4**.

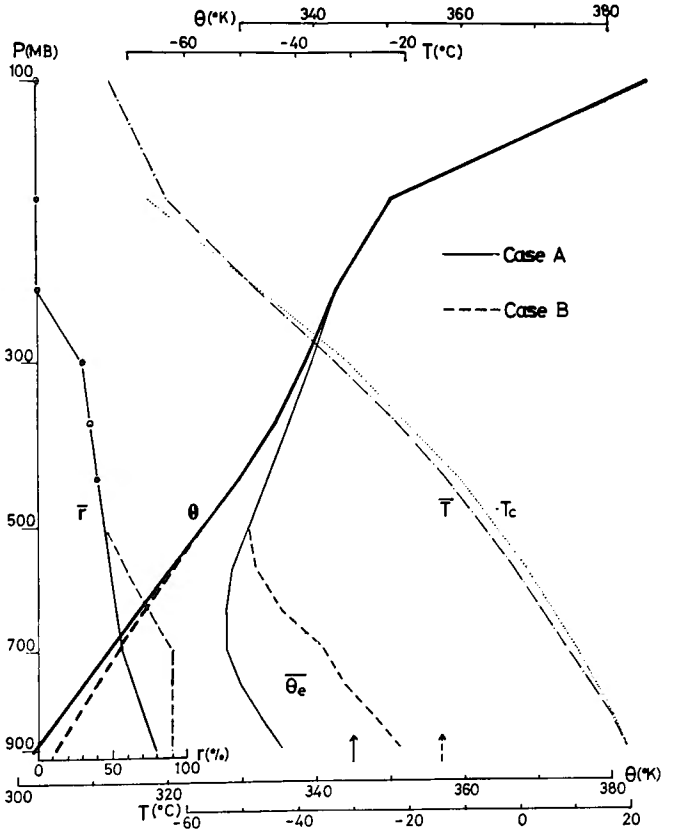

Fig. 2. Basic states of the potential temperature (Θ), the relative humidity ($\bar{r}$) and the equivalent potential temperature ($\bar{\theta}_e$) in Case A (solid lines) and Case B (dashed lines). Arrows indicate θ_e of the cloud. Temperature of environmental air ($\overline{T}$) and cloud air (T_c) are drawm for Case A.

2.2 Boundary conditions and initial conditions

The upper boundary of the atmospheric layer concerned is assumed to be at 100-mb level and the lower boundary is at 900-mb level which is assumed to be the

top of the planetary boundary layer. The boundary conditions for ω are

$$\omega_T = 0, \tag{2.7}$$

and

$$\omega_B = -A\zeta_B, \tag{2.8}$$

where $A = \rho_B g\sqrt{K_z/2f}\sin 2\alpha$. ζ, ρ, g, K_z and α are the perturbation vorticity, the air density, the acceleration of gravity, the coefficient of vertical eddy viscosity and the angle between isobar and wind direction at the anemometer level respectively. Subscripts T and B indicate the values at the upper and the lower boundaries respectively. Eq. (2.8) gives the frictionally induced vertical velocity at the top of the Ekman layer (Brunt [1941], Charney and Eliassen [1949]). The lateral boundary conditions are assumed to be cyclic.

The sinusoidal perturbations of u and v which are expressed as

$$u = U_0 \sin\left(\frac{2\pi x}{L_0} + \varphi_u\right), \tag{2.9}$$

$$v = V_0 \sin\left(\frac{2\pi x}{L_0} + \varphi_v\right), \tag{2.10}$$

are superimposed on the basic state initially, where U_0 and V_0, φ_u and φ_v are the amplitudes and the phase angles of u and v respectively. They satisfy the relation,

$$\int_{p_T}^{p_B} \frac{\partial u}{\partial x} dp = A\frac{\partial v_B}{\partial x}, \tag{2.11}$$

which can be derived from Eqs. (2.4), (2.7) and (2.8).

3. Parameterization of cumulus convection

Two schemes parameterizing cumulus convection, *i.e.* "penetrative moist convection" and "convective adjustment" are compared with each other by applying them to the model atmosphere.

3.1 Penetrative moist convection (PMC)

This hypothesis originally developed by Ooyama [1963, 1969] in the study of tropical cyclone is based on the idea that a) cumulus convection develops wherever there is a conditionally unstable deep layer with horizontal convergence in the planetary boundary layer associated with a large-scale motion, and b) an effect of cumulus convection penetrates to the level where the cloud air loses the buoyancy.

(1) *PMC1*

Yamasaki [1968a, b] investigated the dependence of tropical cyclone development on the vertical distribution of heating in the PMC scheme. A total amount of heat released in a vertical air column with unit cross section per unit time was assumed

to be equal to the upward flux of water vapor at the top of the boundary layer and to be distributed to each level following the heating ratio, h,

$$\dot{Q}_c = -hL\tilde{q}\omega_B, \tag{3.1}$$

where $\tilde{q}$ is the specific humidity at the cloud base which is assumed to be equal to the saturation specific humidity at 900-mb. Yamasaki [1968c] assumed the following heating ratio:

$$h = \begin{cases} (T_c - T)/\int_{p_T}^{p_B}(T_c - T)\,dp, & \text{if } \omega_B < 0 \text{ and } T_c > T \\ 0 & \text{, if } \omega_B \geq 0 \text{ or } T_c \leq T, \end{cases} \tag{3.2}$$

where T_c is the temperature in the cloud in which the moist adiabatic process takes place. His model did not include the moisture explicitly. Therefore,

$$\dot{Q} = \dot{q}_c = 0. \tag{3.3}$$

We abbreviate this scheme as PMC1.

(2) *PMC2*

Only the released latent heat due to condensation through cumulus convection is taken into account in PMC1. Actually convective clouds, however, have a function of moisture transport as well. Kuo [1965], Rosenthal [1970] and Sundqvist [1970] proposed a model which includes moisture accumulation due to cumulus convection as well as to large-scale motion. In this scheme the moisture flux through the top of the boundary layer gives rise to heating and moisture accumulation. Formulations similar to that in PMC1 are used concerning vertical distribution of heating and moistening, *i.e.*,

$$\dot{Q}_c = -h_\theta L\tilde{q}\omega_B, \tag{3.4}$$

$$\dot{q}_c = -h_q\tilde{q}\omega_B, \tag{3.5}$$

$$h_\theta = \begin{cases} c_p(T_c - T)/\int_{p_T}^{p_B}\{c_p(T_c - T) + L(q_c - q)\}\,dp, & \text{if } \omega_B < 0 \text{ and } T_c > T \\ 0, & \text{if } \omega_B \geq 0 \text{ or } T_c \leq T, \end{cases} \tag{3.6}$$

$$h_q = \begin{cases} L(q_c - q)/\int_{p_T}^{p_B}\{c_p(T_c - T) + L(q_c - q)\}\,dp, & \text{if } \omega_B < 0 \text{ and } q_c > q \\ 0, & \text{if } \omega_B \geq 0 \text{ or } q_c \leq q, \end{cases} \tag{3.7}$$

where h_θ and h_q are the parameters which indicate the vertical distribution of the rates of heating and moistening respectively, and q_c is the saturation specific humidity in the cloud. This scheme is called PMC2.

3.2 Convective adjustment (CA)

The concept of convective adjustment was introduced into the general circulation model of GFDL (Geophysical Fluid Dynamics Laboratory) by Manabe *et al.* [1964,

1965]. It is based on the assumptions: a) when the lapse rate Γ and the relative humidity r exceeds certain critical values Γ_c and r_c respectively, cumulus convection develops and adjusts the lapse rate and humidity to the neutral value, and if r is less than r_c, dry convection occurs only when Γ is super-adiabatic, and b) the kinetic energy of convection is converted to the thermal energy instantaneously by frictional dissipation and then the static energy is conserved throughout the process.

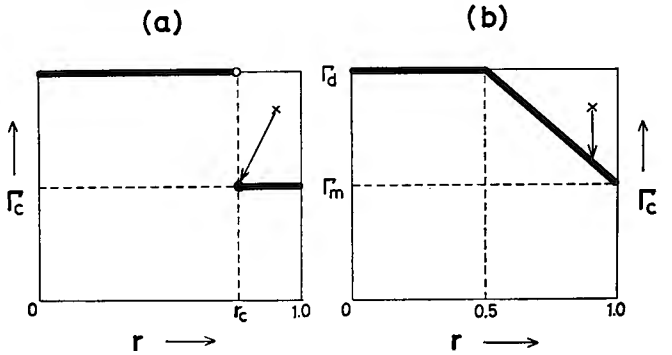

Fig. 3. Relation between relative humidity (r) and critical lapse rate (Γ_c) for CAMS (a) and CAGK (b). An example of adjustment: initial state (cross mark) and adjusted state (top of arrow)

(1) *CAMS (CA100, CA80 and CA60)*

The relation between r and Γ_c in the convective adjustment scheme of the GFDL group is shown in Fig. 3a. When r is less than r_c, Γ_c is the dry adiabatic lapse rate Γ_d and when r is greater than or equal to r_c, Γ_c is the moist adiabatic lapse rate Γ_m. The former adjustment is called "dry convective adjustment" and the latter "moist convective adjustment". The relative humidity is adjusted to r_c in moist convective adjustment.

Convective clouds may be observed in a certain section of the atmosphere where the mean relative humidity does not reach 100% because of the presence of cloud-free regions. This reasons that r_c had better be selected less than 100%, and Miyakoda *et al.* [1969] tested the case when r_c is 80%. We examine three cases of r_c= 100%, r_c=80% and r_c=60% which are denoted by CA100, CA80 and CA60 respectively. All of these three schemes are called CAMS.

(2) *CAGK*

The adjustment scheme of GFDL involves a sort of discontinuity in the relation between r and Γ_c at $r=r_c$ as shown in Fig. 3a. Gadd and Keers [1970] pointed out that this scheme had the disadvantage that unrealistically rapid changes in Γ might be implied and that sudden changes could produce serious defects in computed forecasts. They used a following relation between r and Γ_c as indicated in Fig. 3b.

$$\Gamma c=\begin{cases}\Gamma_d & \text{, for } 0\leq r<r_c \\ \Gamma_d\left(\dfrac{1-r}{1-r_c}\right)+\Gamma_m\left(\dfrac{r-r_c}{1-r_c}\right), & \text{for } r_c\leq r\leq 1,\end{cases} \tag{3.8}$$

where r_c is assumed to be 50%. The relative humidity is kept constant through the procedure of adjustment. Details of this scheme is described by Benwell *et al.* [1971].

An example is illustrated in Fig. 3, indicating that the initial state (cross marked) is converted to the neutral state (the top of the arrow) through the adjustment.

4. Results of numerical experiments

A linear analysis of the governing equations (2.1)~(2.5) yields the solution of a stationary wave and a set of two propagating waves when the PMC scheme is used for a two-layer model. Both the stationary and the propagating waves decay in the model atmosphere of Case A. Case B represents one of the atmosphere in which the stationary wave amplifies with the e-folding time of several days and the propagating waves diminish.

In the first place the dry adiabatic motion ($\dot{Q}, \dot{Q}_c$ and $\dot{q}_c=0$) is examined for a reference. Fig. 4 shows variations of the kinetic energy in the k-th layer ($\bar{K}_k$), the total kinetic energy ($<K>$) and the total energy which is the sum of the total kinetic energy and the total available potential energy ($<K+P_A>$) with time for DRY·A900. Here DRY·A900 denotes the dry adiabatic motion for the atmosphere of Case A on which a perturbation of the wavelength of 900 km is superimposed. Similar abbreviations will be used in the following. For instance, PMC1·B300 denotes the case for which the PMC1 scheme, the model atmosphere of Case B and the perturbation of wavelength of 300 km are used. $\bar{K}_k$, $<K>$ and $<K+P_A>$ are defined as follows.

$$\bar{K}_k=\frac{1}{g}\sum_i\frac{1}{2}(u_{i,k}^2+v_{i,k}^2)\Delta x\Delta p, \tag{4.1}$$

$$<K>=\sum_k \bar{K}_k, \tag{4.2}$$

$$<P_A>=\frac{1}{g}\sum_k\sum_i\left(-\frac{1}{2}\frac{R\pi^*}{\frac{\partial\Theta}{\partial p}^p}\theta_{i,k}'^2\right)\Delta\lambda\Delta p, \tag{4.3}$$

$$<K+P_A>=<K>+<P_A>, \tag{4.4}$$

where

$$\theta_{i,k}'=\theta_{i,k}-\sum_{i=1}^{I}\theta_{i,k}/I, \tag{4.5}$$

and subscripts i and k indicate the i-th grid point in the x-direction and the k-th grid point in the p-direction respectively, I is the total number of grid points in the x-direction and Δx and Δp are the grid distances in the x- and p-directions respectively.

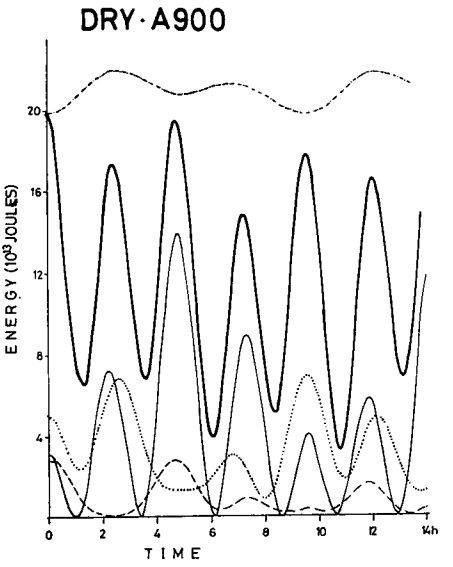

Fig. 4. Time changes of $\bar{K}_1$ (thin solid line), $\bar{K}_4$ (dashed line), $\bar{K}_6$ (dotted line), $<K>$ (thick solid line) and $<K+P_A>$ (dash-dotted line) for the case DRY·A900.

In the dry adiabatic case an inertia-gravity wave whose period coincides with that obtained by the linear analysis of the governing equations is predominant as shown in Fig. 4. The following discussions are made primarily on deviations of the energies defined above from those for the dry adiabatic cases which are denoted by $\Delta<K>$, $\Delta<K+P_A>$ and so forth.

4.1 Comparison of the PMC and CA schemes

Variations of the amount of one-hour precipitation with time are shown in Fig. 5 for the different schemes. The amount of convective precipitation, P_C, is indicated in the upper side of the abscissa and the amount of non-convective precipitation, P_{NC}, in the lower side. P_C is produced from the term $\dot{Q}_c/L$ in Eq. (2.5), while P_{NC} is derived from the term $\dot{Q}/L$. A distinct difference between both the PMC and CA schemes will be observed in P_C. A remarkable feature of the PMC scheme, which appears typically in PMC1, is continuous precipitation without large fluctuation. On the other hand precipitation is intermittent and fluctuates considerably in the CA scheme.

Fig. 6 shows the time changes of $\Delta<K>$ and $\Delta<K+P_A>$ for the same cases as in Fig. 5. In all the schemes the kinetic energies gradually decrease oscillating with a period of the inertia-gravity wave. The total energy in CA decreases like a step function. It is seen that the time when the total energy suddenly decreases coincides with the time when the precipitation occurs. A discussion of these characteristics is made in Section **5**. Variations of $\Delta<K>$ and $\Delta<K+P_A>$ with time in

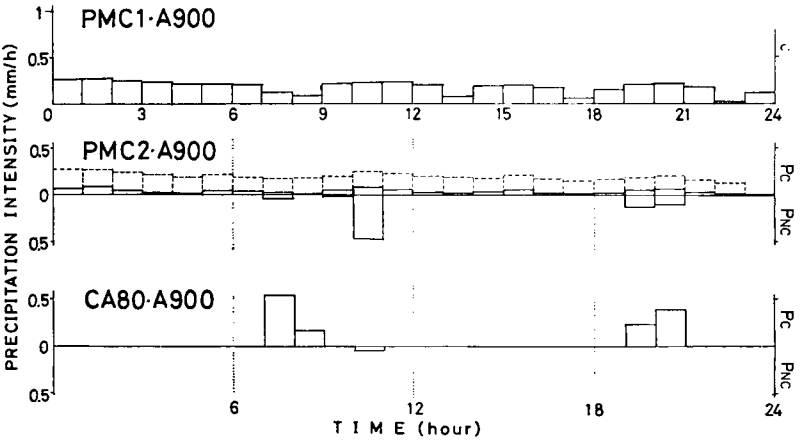

Fig. 5. Amount of one-hour convective precipitation (upper side of abscissa) and non-convective precipitation (lower side of abscissa). The dashed boxes in PMC2 indicate the amount of water vapor supplied from the boundary layer.

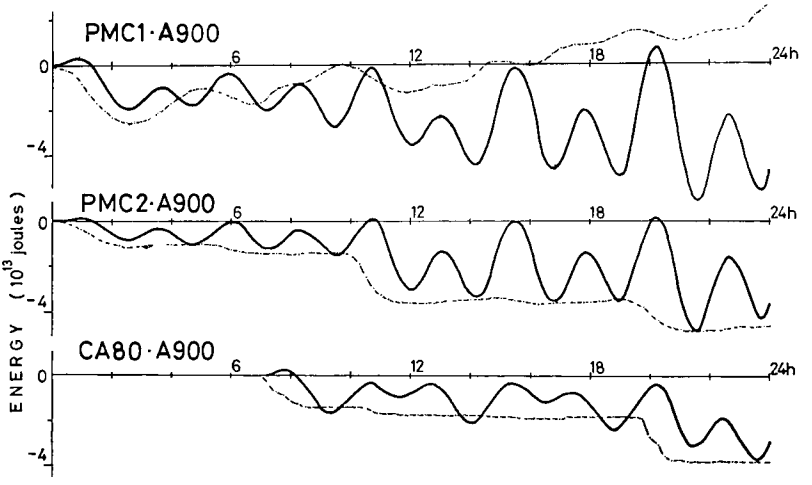

Fig. 6. Variation of $J<K>$ (solid lines) and $J<K+P_A>$ (dash-dotted lines) with time for the case A900.

Case B for each of the schemes are shown in Fig. 7. For the case of PMC1 a stationary wave denoted by the dashed line amplifies with almost the same growth rate as expected by the linear stability analysis. In the other schemes stationary waves amplify with the e-folding time of several hours which is much shorter than that of the stationary wave in PMC1. These unstable waves with the short e-folding time are characterized by a narrow and intensive ascending region compared with the associated descending region so that they may be regarded as thermal convections rather than meso-scale disturbances.

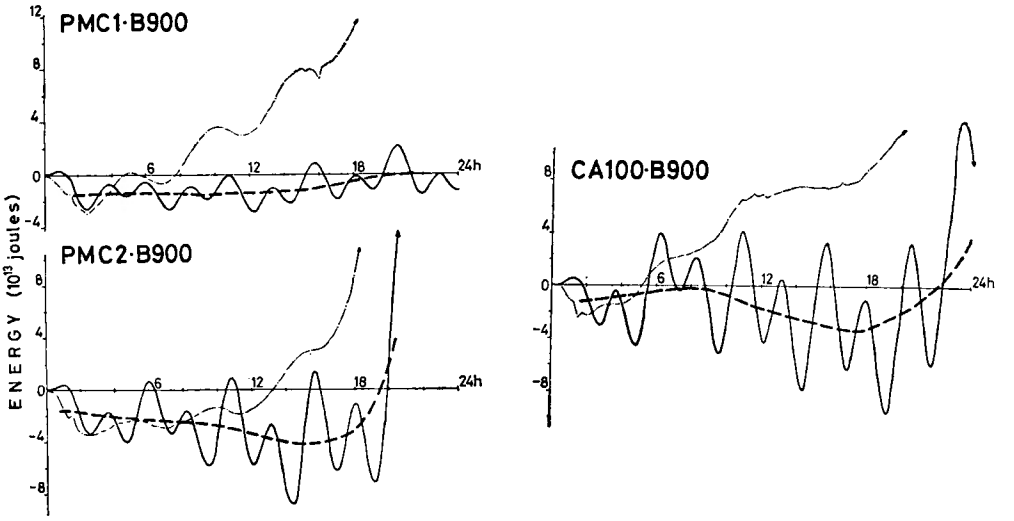

Fig. 7. The same as Fig. 6 except the case B900. J and K of stationary waves are indicated by dashed lines.

The vertical distributions of heating in the cases of A900 and B900 are shown in Figs. 8a and 8b respectively. As anticipated from the definition of heating ratio by Eq. (3.2) and the difference between $\bar{T}$ and T_e shown in Fig. 2, a maximum of the warming appears at a middle or an upper level and the warming expands even into the uppermost layer with stable stratification, while in the CA scheme it is located at a level lower than that in PMC because the mechanism of adjustment acts only in an unstable lower half of the layer and the warming hardly penetrates into upper

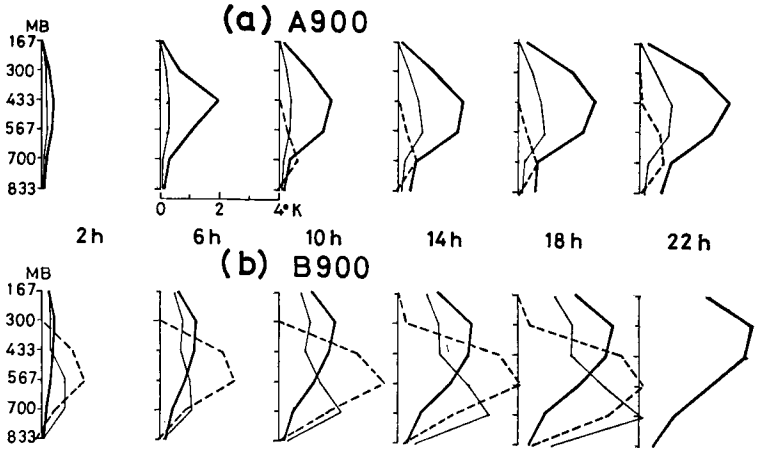

Fig. 8. The deviation of level-mean temperature from the initial state for the cases A900 (upper) and B900 (lower). PMC1 (thick solid lines), PMC2 (thin solid lines) and CAMS (dashed lines) are drawn.

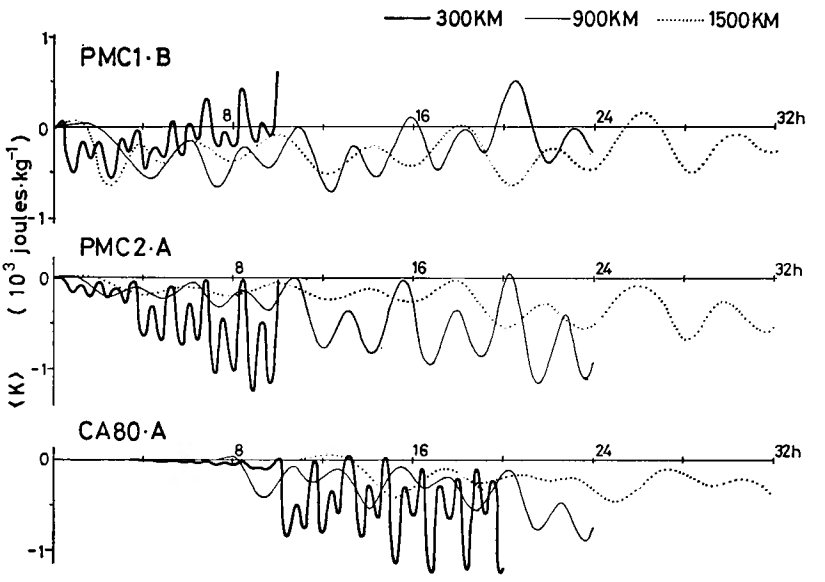

Fig. 9. Variations of $\int\langle K\rangle$ with time for the wavelengths of perturbation of 300 km (thick solid lines), 900km (thin solid lines) and 1500km (dotted lines).

levels as far as during a period of tens of hours which are regarded as time-scale of intermediate-scale perturbations. Note that a maximum warming stays in a low level owing to the non-convective condensation in PMC2·B900.

Fig. 9 shows the time variations of $\int\langle K\rangle$ of perturbations of different wavelengths. An amplifying or damping rate of a perturbation increases as a wavelength decreases for PMC as far as wavelengths are between 150 km and 2000 km. This feature can be found for CA as well, but the dependence of amplifying or damping rate on the wavelength of perturbation is not so much as that for PMC. As is shown in Figs. 5 and 10, the amount of precipitation decreases with time for the CA scheme. This is because there is no net water vapor flux through the top of the boundary layer for the CA scheme and the atmosphere concerned gets dryer by precipitation. It is feasible that the growth rate of perturbations for the CA scheme is reduced by the effect that humidity of the atmosphere is lowered.

4.2 Effect of critical relative humidity in CAMS

The amounts of one-hour precipitation are shown in Fig. 10 for CA100, CA80 and CA60 in the case of A900. The convective precipitation increases and the non-convective one decreases as the critical relative humidity, r_c, becomes lower. More amount of water vapor precipitates out from the system as r_c is lowered. The levels of maximum warming are the same for all the CAMS schemes.

4.3 Production of numerical noises in the CA scheme

As mentioned in Section **3** the CAMS scheme gives rise to a sudden change of the lapse rate and is likely to make a "shock noise". We investigate to what extent

this defect is mitigated by introducing a continuous function such as Eq. (3.8) proposed by Gadd and Keers. Fig. 11 shows the deviations of the x-component of the velocity at the lowest level from the sine function after 12 hours from the initial for B900. A noise of wavelength of $2\Delta\lambda$ appears in the CA100 scheme, while the noise developed in CA100 is mitigated to some extent by using the CAGK scheme. Disturbances of short wavelengths are not observed for the PMC1 scheme.

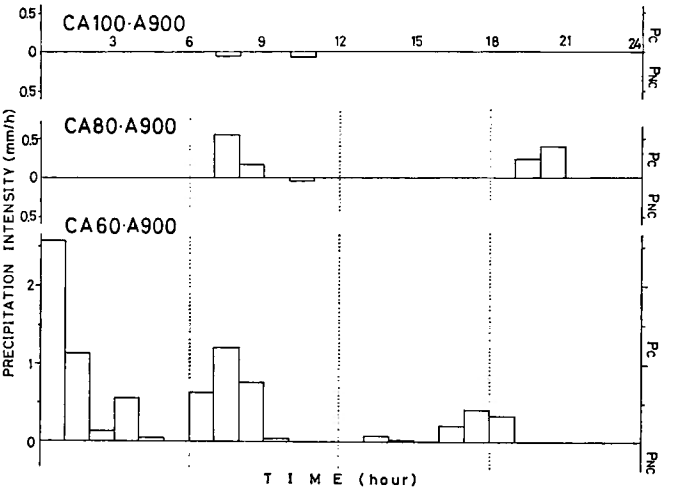

Fig. 10. Time variations of one-hour precipitation for CA100, CA80 and CA60.

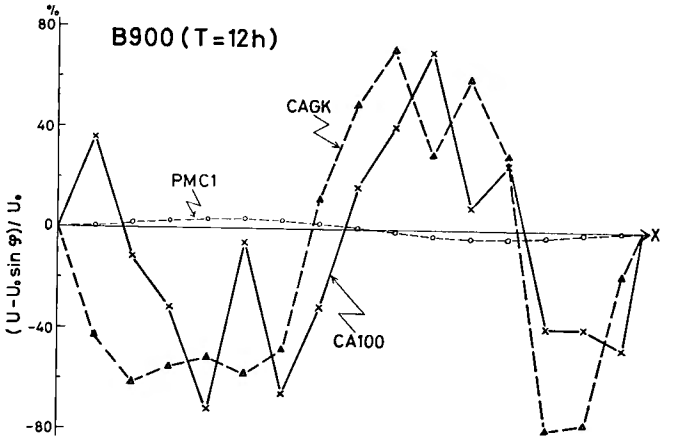

Fig. 11. Deviation of u_{12} from sine function at the time of 12th hour for B900.

5. Remarks

As is seen in Fig. 6, a sudden decrease of total energy coincides with an occurence of precipitation in both the schemes of PMC2 and CA. The non-convective con-

densation of water vapor takes place in the ascending regions where the temperature is lower through adiabatic expansion and the air is saturated with water vapor. The heating in the lower temperature region reduces the horizontal temperature gradient and then decreases the available potential energy. The convective condensation by the CA scheme indicates similar features. Whether the available potential energy is decreased by the non-convective condensation in the actual atmosphere or not remains to be examined for intermediate-scale disturbances concerned here.

Fig. 5 indicates that only about 20% of the amount of water vapor supplied through the top of the boundary layer is converted to heat energy and the rest is accumulated in the free atmosphere, whereas all of the supplied water vapor is used for heat source in the PMC1 scheme. It will be important to analyze how much percentage of supplied water vapor is converted to heat by cumulus convection.

In the CAMS scheme r_c has a significant influence on an evolution of perturbation, especially on the amount of condensattion. However, the most reasonable value of r_c is expected to vary with the grid distance employed as well as with the height and the sort of clouds as mentioned by Smagorinsky [1960]. However, little is known concerning this problem. The relation between r and Γ_c such as Eq. (3.8) in the CAGK scheme is less sensitive to the value of r_c than the CAMS scheme.

From a viewpoint of calculation technique the CAGK scheme seems to be better than the CAMS scheme because of reducing noises which may be produced by numerical processes. It should be mentioned, however, that noises of short wavelengths are unavoidable by the CAGK scheme. Noises thus produced may be suppressed considerably by lateral mixing and by a non-instantaneous adjustment taking account of the life time of the clouds.

Acknowledgments

This study is supported by Funds for Scientific Research from the Ministry of Education. The computations were made with the use of the FACOM 230–60 Computer of the Data Processing Center of Kyoto University.

References

Arakawa, A., A. Katayama and Y. Mintz, 1968; Numerical simulation of the general circulation of the atmosphere, Proceedings of WMO/IUGG Symposium on Numerical Weather Prediction, Tokyo, 1968.

Asai, T. and A. Kasahara, 1967; A theoretical study of the compensating downward motions associated with cumulus clouds, J. Atmos. Sci., **24,** 487–496.

Benwell, G. R. R., A. J. Gadd, J. F. Keers, M. S. Timpson and P. W. White, 1971; The Bushby-Timpson 10-level model on a fine mesh, Scientific Paper No. 32, Meteorological Office, Her Majesty's Stationary Office, London, 59 pp.

Brunt, D., 1941; *Physical and dynamical meteorology,* Univerity Press, Cambridge, 428 pp.

Charney, J. G. and A. Eliassen, 1949; A numerical method for predicting the perturbations of the middle latitude westerlies, Tellus, **1,** 38–54.

Charney, J.G. and A. Eliassen, 1964; On the growth of the hurricane depression, J. Atmos. Sci., **21,** 68–75.

Gadd, A. J. and J. F. Keers, 1970; Surface exchange of sensible and latent heat in a 10-level model atmosphere, Quart. J. R. Meteor. Soc., **96,** 297–308.

Jordan, C. L., 1958; Mean soundings for the West Indies area, J. Meteor., **15,** 91–97.

Kuo, H. L., 1965; On formation and intensification of tropical cyclones through latent heat release by cumulus convection, J. Atmos. Sci., **22,** 40–63.

Manabe, S. and R. F. Strickler, 1964; Thermal equilibrium of the atmosphere with a convective adjustment, J. Atmos. Sci., **21,** 361–385.

Manabe, S., J. Smagorinsky and R. F. Strickler, 1965; Simulated climatology of a general circulation model with a hydrologic cycle, Mon. Wea. Rev., **93,** 769–798.

Miyakoda, S., J. Smagorinsky, R. F. Strickler and G. D. Hembree, 1969; Experimental expended predictions with a nine-level hemispheric model, Mon. Wea. Rev., **97,** 1–76.

Ooyama, K., 1963; A dynamical model for the study of tropical cyclone development, Manuscript for the 43rd annual meeting of the American Meteorological Society, New York, 1963 (unpublished).

————, 1969; Numerical simulation of the life cycle of tropical cyclones, J. Atmos. Sci., **26,** 3–40.

Palmén, E. and C. W. Newton, 1969; *Atmospheric circulation systems,* Academic Press, New York and London, Chap. **2,** 26–66.

Riehl, H. and J. S. Malkus, 1961; Some aspects of hurricane Daisy, 1958, Tellus, **13,** 181–213.

Rosenthal, S. L., 1970; A circularly symmetric primitive equation model of tropical cyclone development containing an explicit water vapor cycle, Mon. Wea. Rev., **98,** 643–663.

Smagorinsky, J., 1960; On the dynamical prediction of large-scale condensation by numerical methods, Geophysical Monograph, No. 5, American Geophysical Union, 71–78.

Sundqvist, H., 1970; Numerical simulation of the development of tropical cyclones with a ten-level model, Part I, Tellus, **22,** 359–390.

Yamasaki, M., 1968a; Numerical simulation of tropical cyclone development with use of primitive equations, J. Meteor. Soc. Japan, **46,** 178–201.

————, 1968b; A tropical cyclone model with parameterized vertical partition of released latent heat, J. Metor. Soc. Japan, **46,** 202–214.

————, 1968c; Detailed analysis of a tropical cyclone simulated with a 13-layer model, Papers Meteor. Gorphys., **19,** 559–585.